

Distinguishing cusp effects and near-threshold-pole effects

Zhi-Yong Zhou^{1,2,*} and Zhiguang Xiao^{3,2,†}

¹*Department of Physics, Southeast University, Nanjing 211189, P. R. China*

²*State Key Laboratory of Theoretical Physics, Institute of Theoretical Physics,
Chinese Academy of Sciences, Beijing 100190, China*

³*Interdisciplinary Center for Theoretical Study,
University of Science and Technology of China, Hefei, Anhui 230026, China*

(Dated: November 10, 2018)

Abstract

We make use of a unitarized coupled-channel model to analyze the mass distribution data of final states in production processes of $X(4260)$. By analyzing the analytical structures of the decay amplitudes, we find that the line shape of $Z_c(3900)$ signal is related to the combined effect of a pair of near-threshold “shadow” poles and the $(D\bar{D}^*)^\pm$ thresholds, in which the third-sheet pole might provides a dominant contribution. As all the coupled channels effects are tuning off, the trajectories of these two poles suggest that the $Z_c(3900)$ might originate from the attractive interaction of $(D^*\bar{D}^*)^\pm$ through a long-distance interaction, *e.g.* π -exchange interaction, as a “deuteron-like” state. There is no nearby pole structure corresponding to the $Z_c(4025)$ signal in the $(D^*\bar{D}^*)^\pm$ mass distribution.

* zhouzhy@seu.edu.cn

† xiaozg@ustc.edu.cn

Dynamical origins of near-threshold structures are under heavy debates since more and more such signals are observed in experimental explorations [1]. Among others, the ones in the charged channels with heavy quarkonium final states are of specific interest in both theoretical and experimental investigations because of their possible exotic nature. If these structures, dubbed Z_c 's or Z_b 's, are really produced by resonant states, they contain at least four quark components in exotic forms of matter such as hadronic molecules, quark-gluon hybrids, tetraquarks, and some others [2].

Intense experimental searches for near-threshold charged exotic candidates started from the observations of $Z_b(10610)$ and $Z_b(10650)$ structures by Belle in $e^+e^- \rightarrow \Upsilon(5S) \rightarrow \Upsilon(nS)\pi^+\pi^-$ and $\Upsilon(5S) \rightarrow h_b(nP)\pi^+\pi^-$ processes by analyzing the final $\Upsilon(nS)\pi^\pm$ or $h_b(nP)\pi^\pm$ mass distributions [3]. The $Z_c(3900)$ was reported by BES in $e^+e^- \rightarrow X(4260) \rightarrow J/\psi\pi^+\pi^-$ [4], and then $Z_c(3885)$ in $e^+e^- \rightarrow (D\bar{D}^*)^\mp\pi^\pm$ [5], $Z_c(4025)$ in $e^+e^- \rightarrow (D^*\bar{D}^*)^\mp\pi^\pm$ [6]. Since these signals appear just near some open-flavor thresholds, interpreting them as resonances are doubted by some groups and they suggested the signals be caused by the effects of threshold cusps (see references [7, 8] for example). In fact, the experimental data could be reproduced through rescattering models without introducing new states [9, 10]. However, this mechanism of pure cusp effects is challenged by Ref. [11], in which the authors criticized the calculations mentioned above for not including the higher-order contributions which may lead to significant deviations from the lowest-order result. They presented that a numerical calculation incorporating higher-order perturbation series in an elastic channel could dynamically generate a bound state right below the threshold. Recently, the author of Ref.[8] improved his cusp model and claimed that it is not necessary to introduce poles to explain the signals of $Z_c(3900)$ and $Z_c(4025)$ even after the higher-order contributions are included [12]. This debate highlights the importance of determining the properties of a near-threshold peak signal and also urges us to find a general method to distinguish the cusp effect and the near-threshold-pole effects as a reference for future experimental exploration.

In this paper, we adopt a coupled-channel model in which the unitarity of the amplitudes is respected and the analytical structures of the amplitudes could be easily analyzed. The contributions from all the relevant two-body hadron loops can be taken into account and all the coupled processes could be studied simultaneously. We apply this scheme to study the mass distribution data of different final states, $J/\psi\pi^\pm$, $(D\bar{D}^*)^\pm$, and $(D^*\bar{D}^*)^\pm$ in the production processes of e^+e^- collisions around 4.26GeV at the same time, and the experi-

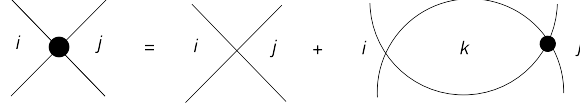


FIG. 1. A pictorial representation of the iterative equation, where the “ i ”, “ j ”, and “ k ” denote the coupled channels. The cross point represents the bare contact interaction and the solid dots represent the full four-point interactions.

mental data could be reproduced in a perfect quality with fewer parameters than those in the experimental line-shape analyses. The numerical results of the best fit demonstrate that the $Z_c(3900)$ signal is found to be generated by a combined effect of two near-threshold poles and the $(D\bar{D}^*)^\pm$ threshold, however, there is no pole corresponding to the $Z_c(4025)$ signal in the $(D^*\bar{D}^*)^\pm$ mass distribution data. This scheme could be easily generalized in other experimental analyses to determine the possible properties of near-threshold structures.

We first explain the basic concepts and the setup of the model briefly. The related experimental information mainly come from production processes, but, due to crossing symmetry, the Lorentz invariant amplitude in a decay process $\mathcal{M}(A(P) \rightarrow B(p_1) + C(p_2) + D(p_3))$ is the analytical continuation of that in a scattering process $\mathcal{M}(A(P) + \bar{D}(k) \rightarrow B(p_1) + C(p_2))$, where \bar{D} represents the antiparticle of D and the four-momentum $k = -p_3$, and vice versa. In other words, they are the same function of the Mandelstam variables, $s = (p_1 + p_2)^2$, $t = (p_1 + p_3)^2$, and $u = (p_2 + p_3)^2$, defined in different physical regions.

We can define a simple factorization form for the two-body scattering partial-wave T amplitude in “Argand Units” in a matrix form as

$$T = G^\dagger \Sigma G, \quad (1)$$

where $G = \text{diag}\{G_1(s), G_2(s), \dots\}$, and $G_n(s) = \sqrt{\rho_n(s)} f_n(s) \theta(s - s_{th,n})$ similar to the Unitarized Quark Model (UQM) [13]. $\rho_n(s)$ is the kinematic factors and is represented as $\rho_n(s) = 2k_n(s)/\sqrt{s}$ where $k_n(s)$ is the three-momenta of two particles in the center-of-mass (CM) frame of the n -th channel. $f_n(s)$ is a simple gaussian form factor defined as $f_n(s) = \exp[-k(s)^2/2k_0^2]$ where $\beta = 1/k_0$ could be regarded as the interaction range of two particles in the channel and this form factor also serves to regularize the ultra-violet divergence in the latter calculation. $\theta(s - s_{th,n})$ is a unit-step function and $s_{th,n}$ is the CM energy square of the n -th threshold. The matrix element Σ_{ij} represents the full partial-wave

amplitude excluding the incoming and outgoing kinematic factors, form factors, and the unit-step functions in $i \rightarrow j$ process. Unlike in the UQM, we will not introduce s -channel bare “seed” states in the Σ function here which means that the poles of the amplitude in our later analysis are all dynamically generated from the coupled-channel interactions. If the s -channel contribution is dominant, as in the processes discussed in this paper, which involve transitions of heavy quark pairs but no annihilations of them, the Σ satisfies an iterative equation

$$\Sigma = \lambda + \lambda \Pi \Sigma, \quad (2)$$

where the matrix element λ_{ij} represents the effective contact interaction strength between the i -th and j -th channels including the bare interaction coefficient, polarization summation factors, and Clebsh-Gordan coefficients in the couplings of angular momenta. $\Pi = \text{diag}\{\Pi_1(s), \Pi_2(s), \dots\}$ where $\Pi_i(s)$ is the hadron loop integral function with intermediate states of the i -th channel. Eq.(2) could be represented pictorially as in Fig.1, which means that contributions from all kinds of bubble chains have been summed up, and it could be viewed as a simplification of the Lippmann-Schwinger equation as in Ref. [14, 15].

The coupled-channel unitarity relation

$$(T - T^\dagger)/2i = TT^\dagger \quad (3)$$

leads to

$$\frac{1}{2i}(G^\dagger \Sigma G - G^\dagger \Sigma^\dagger G) = G^\dagger \Sigma G G^\dagger \Sigma^\dagger G, \quad (4)$$

which requires

$$\text{Im}\Sigma^{-1} = -GG^\dagger. \quad (5)$$

From Eq.(2), the inverse matrix of Σ is represented as

$$\Sigma^{-1} = \lambda^{-1}(I - \lambda\Pi), \quad (6)$$

where I is the unit matrix. Thus,

$$\text{Im}\Pi = GG^\dagger, \quad (7)$$

which means that the imaginary part of $\Pi_n(s)$ function is $\text{Im}\Pi_n(s) = \rho_n(s)f_n^2(s)\theta(s - s_{th,n})$.

The real part of $\Pi_n(s)$ function is determined through a dispersion relation

$$\text{Re}\Pi_n(s) = \frac{1}{\pi} \mathcal{P} \int_{s_{th,n}}^{\infty} \frac{\text{Im}\Pi_n(s)}{z - s} dz, \quad (8)$$

where $\mathcal{P} \int$ denotes the Cauchy principal integration.

Now, we have a unitarized partial-wave coupled-channel scattering amplitude with all higher-order loops summed up, in which no s -channel bare state is introduced since λ_{ij} 's only represent the contact interactions of the two channels. But, the resonances or bound states could be produced dynamically, if the interaction strengths are strong enough. The poles of the amplitude, evaluated by the zero points of determinant of $(I - \lambda\Pi)$, can appear on the real axis of the first Riemann sheet for bound states or in the complex s -plane on the other non-physical sheets for resonances.

The pole structures of the amplitude could be analyzed by analytically continuing the amplitude into the complex s -plane as widely discussed in the literature [13, 16, 17]. Every physical cut will double the number of Riemann sheets in the analytical continuation, which means that there are 2^n Riemann sheets for an n -channel amplitude. To find the poles on the closest Riemann sheet attached to the physical region, one need to analyze the analytic structure of $\Pi_n(s)$ in this model. One can evaluate the $\Pi_n(s)$ on the physical sheet by combining Eq.(5) and Eq.(8) and analytically continue it to the complex plane and to the other sheets. Only the poles on the closest Riemann sheet attached to the physical region significantly influence the experimental data in a certain physical region between two sequential thresholds. For example, in the region between $s_{th,1}$ and $s_{th,2}$, one should investigate the singularities of the amplitude near this region on the second Riemann sheet. In the region between $s_{th,2}$ and $s_{th,3}$, one should study that of the third sheet, and so forth.

The picture of this model is clear and easy to understand. In the case that there is only one channel (an elastic case), when the bubble chains are summed up, a term $(1 - \lambda\Pi(s))$ will appear in the denominator of the amplitude. When the interaction is attractive and strong such that λ is larger than $1/\Pi(s_{th})$, a bound state pole below the threshold appears on the real axis of the first Riemann sheet. However, as the coupling becomes weaker, the bound state pole will move across the threshold to the second sheet and become a virtual state pole. While the interaction is repulsive, there is no bound state pole or narrow resonance pole. When more coupled channels are included, these poles usually move to the complex s -plane and become resonance poles.

The experimental data we analyze include the mass distributions of the final states in the processes of $e^+e^- \rightarrow X(4260) \rightarrow J/\psi\pi^+\pi^-$, $(D\bar{D}^*)^\pm\pi^\mp$, and $(D^*\bar{D}^*)^\pm\pi^\mp$. The partial-wave decay amplitude could be represented by the formula above with the scattering kinematic

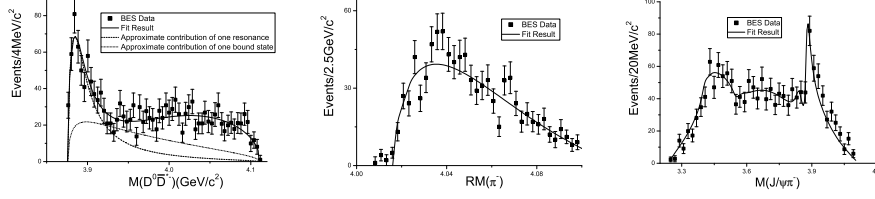


FIG. 2. Fitted curves (Solid lines) are compared with the mass distribution data of $D^0 \bar{D}^{*-}$ [5], $(D^* \bar{D}^*)^+$ represented by the π^- recoil mass spectrum [6], and $J/\psi \pi^-$ [4] from the BES group. The dashed line in the first graph represents the contribution of a second-sheet pole at $(3.875 \pm 0.016i \text{ GeV})^2$, and the dotted line in the first graph represents that of a bound state pole at $(3.846 \text{ GeV})^2$ up to normalizations, as mentioned in the text.

factors removed. There exist four coupled channels, *i.e.* $J/\psi \pi^\pm$, $(D \bar{D}^*)^\pm$, $(D^* \bar{D}^*)^\pm$, and $X(4260) \pi^\pm$, from the lowest threshold to the highest one, and we can define them to be channel “1”, “2”, “3”, and “4”, respectively. The $X(4260) \pi^\pm$ channel is always virtual but it provides a background contribution in principle. Since all of the four channels could transit into each other through S -wave, the higher partial waves are assumed to be small so that we omit their contributions in the calculation. If every two of them do not couple to each other by the s -channel resonance exchange, the effective interactions are represented by coupling constants, λ_{ij} s, only ten of which are independent for the time reversal symmetry. Care must be taken that in the $X(4260) \rightarrow J/\psi \pi^+ \pi^-$ process, due to the s - t symmetry, the invariant amplitude has a contribution from t -channel rescattering as

$$\mathcal{M}(s, t, u) \propto \mathcal{A}_s(s) + \mathcal{A}_t(\Delta - s - u), \quad (9)$$

where $\Delta = m_{X(4260)}^2 + m_{J/\psi}^2 + 2m_\pi^2$, while, in $X(4260) \rightarrow (D \bar{D}^*)^\mp \pi^\pm$ and $X(4260) \rightarrow (D^* \bar{D}^*)^\mp \pi^\pm$ processes, only s -channel contributions are considered.

The total 14 fitted parameters include ten coupling constants, the regularization parameter k_0 , and three normalization factors. The data sets of mass distribution we choose are those of $J/\psi \pi^-$, $(D \bar{D}^*)^-$, $(D^* \bar{D}^*)^+$ [4–6]. The fits to other data sets also leads to similar physical conclusions, so we do not show the corresponding fit results here. The best fit for the data sets we choose presents a perfect reproduction of the experimental information with $\frac{\chi^2}{d.o.f} = \frac{125.9}{60+33+43-14} \simeq 1.03$, as shown in Fig.2. To reduce the time consumption of the numerical calculation, we fixed the k_0 parameter in values between 0.3 and 0.4 in span

of 0.01, and found the minimum of the χ^2 corresponds to $k_0 = 0.36$. The fitted coupling constants are listed in the following:

$$\begin{aligned}
\lambda_{11} &= -41.5 \pm 0.5, \lambda_{12} = -28.0 \pm 1.3, \lambda_{13} = 2.5 \pm 0.4, \\
\lambda_{14} &= -12.9 \pm 1.7, \lambda_{22} = -30.2 \pm 4.0, \lambda_{23} = -8.6 \pm 0.8 \\
\lambda_{24} &= -28.6 \pm 3.7, \lambda_{33} = 71.9 \pm 1.1, \lambda_{34} = -8.9 \pm 1.3 \\
\lambda_{44} &= 138.7 \pm 1.6.
\end{aligned} \tag{10}$$

With the procedure to extract the pole structure described above, one can easily find the nearby pole close to the physical region. The second-sheet poles are searched for near the region between $s_{th,1}$ and $s_{th,2}$, the third-sheet ones near the region between $s_{th,2}$ and $s_{th,3}$, and the fourth-sheet ones near the region between $s_{th,3}$ and $s_{th,4}$. A second-sheet pole below the $D\bar{D}^*$ threshold and a third-sheet pole just on the $D\bar{D}^*$ threshold are found and the locations on the complex s -plane are

$$\begin{aligned}
\sqrt{s^{II}} &= 3.846 \pm 0.019i \text{ GeV}, \\
\sqrt{s^{III}} &= 3.875 \pm 0.016i \text{ GeV}.
\end{aligned} \tag{11}$$

However, there is no near-threshold pole close to the $D^*\bar{D}^*$ threshold. So the best fit of this model prefers a solution with near-threshold poles to produce the $Z_c(3900)$ signal, which is different from the conclusion of Ref.[12].

Until now, there is no method to extract the contribution of every single pole in a multi-channel amplitude, but we propose that the peak structure in the $D\bar{D}^*$ mass distribution is mainly contributed by the third-sheet pole by the following arguments. If the lowest $J/\psi\pi$ threshold is omitted, the numbers of Riemann sheet will reduce to 8. Then, the third sheet becomes the second sheet and the second sheet becomes the first sheet that the s^{II} is supposed to be mimicked by a real bound state at about $(3.846 \text{ GeV})^2$ [18] and s^{III} a second-sheet resonance. In Ref.[19], a rigorous formula of unitary scattering amplitude with only a virtual state or a bound state in an elastic scattering is shown as

$$T_{virtual/bound}(s) = \frac{\pm \frac{s}{s-s_L} \sqrt{\frac{s_0-s_L}{s_R-s_0}}}{1 \mp i\rho(s) \frac{s}{s-s_L} \sqrt{\frac{s_0-s_L}{s_R-s_0}}}, \tag{12}$$

where $s_L = (m_1 - m_2)^2$, $s_R = (m_1 + m_2)^2$, with m_1 and m_2 denoting the masses of the two scattering particles, and s_0 being the mass squared of the virtual/bound state. The

amplitude of a resonance in an elastic scattering is

$$T_{resonance}(s) = \frac{s G(z_0)}{M^2(z_0) - s - i\rho(s)sG(z_0)}, \quad (13)$$

where

$$\begin{aligned} M^2(z_0) &= \text{Re}[z_0] + \frac{\text{Im}[z_0]\text{Im}[z_0\rho(z_0)]}{\text{Re}[z_0\rho(z_0)]}, \\ G(z_0) &= \frac{\text{Im}[z_0]}{\text{Re}[z_0\rho(z_0)]}, \end{aligned} \quad (14)$$

and z_0 means the pole position on the second sheet. A second-sheet pole at $3.875 \pm 0.016 \text{ GeV}$ will contribute a peak around 3.885 GeV , consistent with the experimental data, while a bound state at 3.846 GeV only contributes a mild enhancement above the threshold as shown in Fig.2.

The negative sign of λ_{22} in this model means a repulsive interaction of $D\bar{D}^*$, which implies that the state might not be formed by $D\bar{D}^*$. But the $D^*\bar{D}^*$ might be attractive for a large positive λ_{33} . By gradually decreasing the interaction strengths between different channels, *i.e.* the non-diagonal elements of the λ matrix, which means that the different channels are decoupled with others, the two poles mentioned above move to the same location at real axis on different Riemann sheets, $\sqrt{s} = 3.862 \text{ GeV}$, which is just the pole position of a bound state of $D^*\bar{D}^*$ in the elastic case. The pole trajectory means that these two poles are just two “shadow” poles originated from the strong attraction between $D^*\bar{D}^*$. [16] It seems that the binding energy of the $D^*\bar{D}^*$ system is about 140 MeV , larger than the usual expected value, but it is not in conflict with the heavy quark chiral perturbation calculation. In fact, Ref.[20] has exhibited the possibility of binding the vector meson pair through a long-distance π -exchange potential in heavy quark limit. Furthermore, numerical calculations in Ref.[21] show that the binding energy of $D^*\bar{D}^*$ through π -exchange could be large up to $90_{-50}^{+100} \text{ MeV}$.

The large positive λ_{44} also produce a spurious bound state below the $J/\psi\pi$ threshold which could be an artifact of this model, but it does not affect the physical conclusions for the reasons below. Since the $X(4260)\pi$ threshold is always virtual in the decay process, this channel only contributes to the background of the experimental data. In fact the background could come from a lot of other effects such as t -channel contributions and higher partial waves and so on. In the fitting process, λ_{44} is freely running and this channel could absorb all the background effects. As a result, λ_{44} should not be taken seriously as the coupling of this

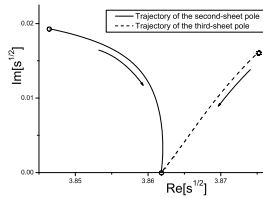


FIG. 3. Trajectories of the second-sheet pole and the third-sheet one as all the coupled channel effects are being switched off.

channel. So, it is not surprising that in this channel there could be a faraway pole which serves to simulate all the background effects in the physical data region.

To conclude, utilizing a model summing up all the two-hadron bubble-chain contributions and respecting coupled-channel unitarity, we analysed the three invariant mass distributions of $J/\psi\pi^\pm$, $(D\bar{D}^*)^\pm$ and $(D^*D^*)^\pm$ simultaneously in the e^+e^- production processes around 4.260GeV. The numerical result prefers that the $Z_c(3900)$ signal to be contributed by a pair of near-threshold poles, of which the third-sheet one contribute dominantly. These poles might originate from the strong interaction between $D^*\bar{D}^*$ through long-distance π -exchange interactions, which is similar to the deuteron state. There is no pole structure corresponding to the $Z_c(4025)$ signal in $D^*\bar{D}^*$ mass distribution. Moreover, the unitarized scheme may be generalized to analyze other near-threshold structures.

Note: When the paper is completed, we noticed a related work is just released in arXiv, in which the author also found a second-sheet pole at $3876 + i5\text{MeV}$ in studying elastic $D\bar{D}^*$ scattering [22].

ACKNOWLEDGMENTS

Helpful discussions with Hai-Qing Zhou are appreciated. This work is supported by the National Natural Science Foundation of China under grant No.11375044, 11105138, and 11235010. Z.X is also partly supported by the Fundamental Research Funds for the Central Universities under grant No.WK2030040020.

[1] K. Olive *et al.* (Particle Data Group), Chin.Phys. **C38**, 090001 (2014).

- [2] N. Brambilla, S. Eidelman, B. Heltsley, R. Vogt, G. Bodwin, *et al.*, Eur.Phys.J. **C71**, 1534 (2011), arXiv:1010.5827 [hep-ph].
- [3] A. Bondar *et al.* (Belle), Phys.Rev.Lett. **108**, 122001 (2012), arXiv:1110.2251 [hep-ex].
- [4] M. Ablikim *et al.* (BESIII), Phys.Rev.Lett. **110**, 252001 (2013), arXiv:1303.5949 [hep-ex].
- [5] M. Ablikim *et al.* (BESIII), Phys.Rev.Lett. **112**, 022001 (2014), arXiv:1310.1163 [hep-ex].
- [6] M. Ablikim *et al.* (BESIII), Phys.Rev.Lett. **112**, 132001 (2014), arXiv:1308.2760 [hep-ex].
- [7] D. Bugg, Europhys.Lett. **96**, 11002 (2011), arXiv:1105.5492 [hep-ph].
- [8] E. Swanson, Phys.Rev. **D91**, 034009 (2015), arXiv:1409.3291 [hep-ph].
- [9] X. Wang, Y. Sun, D.-Y. Chen, X. Liu, and T. Matsuki, Eur.Phys.J. **C74**, 2761 (2014), arXiv:1308.3158 [hep-ph].
- [10] D.-Y. Chen, X. Liu, and T. Matsuki, Phys.Rev. **D88**, 036008 (2013), arXiv:1304.5845 [hep-ph].
- [11] F.-K. Guo, C. Hanhart, Q. Wang, and Q. Zhao, Phys.Rev. **D91**, 051504 (2015), arXiv:1411.5584 [hep-ph].
- [12] E. Swanson, (2015), arXiv:1504.07952 [hep-ph].
- [13] N. A. Tornqvist, Z.Phys. **C68**, 647 (1995), arXiv:hep-ph/9504372 [hep-ph].
- [14] N. Kaiser, P. Siegel, and W. Weise, Nucl.Phys. **A594**, 325 (1995), arXiv:nucl-th/9505043 [nucl-th].
- [15] J. Oller and E. Oset, Nucl.Phys. **A620**, 438 (1997), arXiv:hep-ph/9702314 [hep-ph].
- [16] R. J. Eden and J. R. Taylor, Phys. Rev. **133**, B1575 (1964).
- [17] Z.-Y. Zhou and Z. Xiao, Phys.Rev. **D83**, 014010 (2011), arXiv:1007.2072 [hep-ph].
- [18] There is no resonance on the first Riemann sheet for the reason of causality.
- [19] H. Zheng, Z. Zhou, G. Qin, Z. Xiao, J. Wang, *et al.*, Nucl.Phys. **A733**, 235 (2004), arXiv:hep-ph/0310293 [hep-ph].
- [20] A. V. Manohar and M. B. Wise, Nucl.Phys. **B399**, 17 (1993), arXiv:hep-ph/9212236 [hep-ph].
- [21] M. P. Valderrama, Phys.Rev. **D85**, 114037 (2012), arXiv:1204.2400 [hep-ph].
- [22] J. He, arXiv:1505.05379 [hep-ph].